

Fault location in active distribution networks by means of the continuous-wavelet analysis of fault-originated high frequency transients

**A. BORGHETTI, M. BOSETTI,
C.A. NUCCI*, M. PAOLONE
UNIVERSITY OF BOLOGNA
ITALY**

**A. ABUR
NORTHEASTERN UNIVERSITY
USA**

SUMMARY

The first aim of the paper is the characterization of fault-originated transients in power distribution networks as a function of the fault location and of the measurement point. Both fault location and of the measurement point are indeed correlated to the position of the faulted branch and of the fault location through the paths covered by travelling waves originated by the fault event.

The second aim of the paper is the identification of these paths, which is of importance for the development of fast and reliable fault location procedure. To this aim, the paper illustrates an algorithm, based on the continuous wavelet analysis of fault-originated transients, that allows for a successful identification of the continuous frequency spectrum of fault transients. The knowledge of that spectrum is then used to identify characteristic frequencies directly correlated to the previously mentioned paths and, therefore, to the fault location.

The paper also presents the structure of a first prototype of fault locator, which implements the proposed procedure. Finally, experimental tests aimed at verifying the performances of that prototype are presented and the results discussed.

KEYWORDS

Fault location – fault transients – distribution networks – continuous wavelet transform.

1. INTRODUCTION

The accurate fault location in medium voltage distribution networks is one of the aspects having a major impact on the quality of service in terms of duration of interruptions when permanent faults occur. Moreover, switching transients associated to both fault location techniques and subsequent manoeuvres for service restoration reconfiguration, may also affect power quality of the distribution system [1]. Additionally, the increasing diffusion of distributed generation calls for accurate and fast fault location procedures aimed at minimizing the network service restoration time and, consequently, minimizing the non-supplied power of this type of generation.

Various procedures for fault location assessment are described in the literature on the subject (e.g. [2]). Some procedures analyze pre and post-fault voltage and currents from their steady state values (e.g. [3-5]), whilst others are based on the analysis of fault-originated electromagnetic transients, (i.e. travelling waves generated by the fault itself, e.g. [6-10]).

It is worth noting that the presence of dispersed generation in distribution networks can affect the accuracy of fault location procedures based on the analysis of steady-state voltage and currents. For these reasons, procedures that belong to the second of the above mentioned categories may be less influenced by the presence of dispersed generation.

In this respect, the paper aims at discussing the accuracy of a fault location procedure based on a combined use of the methods presented in [8,9] and [11,12]. In particular, in [11,12] such a procedure is based on the wavelet analysis of fault-originated electromagnetic transients performed by applying the continuous wavelet transformation (CWT) with specific mother wavelets inferred from the voltage transient waveforms. The relevant analysis is aimed at identifying characteristic frequencies associated to the faulted branch and to the fault location [12,13]. Whilst in [11,12] the characteristic frequencies are estimated by means of a CWT analysis of the transient waveforms only in frequency domain, in order to improve the fault location accuracy the procedure that here is presented extends such an analysis to both time [8,9] and frequency CWT decompositions.

The structure of the paper is the following: section 2 illustrates the characteristics of the electromagnetic transients triggered by the fault occurrence and the relevant correlations with the network topology; section 3 discusses the use of the wavelet analysis, with particular reference to the continuous transform used to identify the characteristic frequencies of the transient signal spectrum that are correlated to the fault location; section 4 describes the structure of a fault location algorithm as well as its implementation into a specific prototype which experimental characterization is also presented and discussed.

2. ELECTROMAGNETIC TRANSIENTS ASSOCIATED TO FAULTS IN RADIAL DISTRIBUTION NETWORKS

A fault event into a power system can be associated to an injection in the power system itself of a step wave triggered by the fault occurrence. The fault-generated step wave travels along the lines of the network and gets reflected in correspondence of the line extremities which are characterized by reflection coefficients whose values depend to the line surge impedances and the impedances of the connected power components. In particular, the line extremities can be grouped into three categories, namely: line terminations with power transformers, junctions among lines, and the fault location. For each of these boundary conditions the following assumptions can be reasonably made:

- extremities where a power transformer is connected can be assumed, for the traveling waves, as open circuits, and therefore the relevant reflection coefficient is close to +1; indeed fault-originated travelling waves are characterized by a spectrum with high-

frequency components for which the input impedance of power transformers is generally dominated by a capacitive behavior [14];

- extremities that correspond to a junction between more than two lines are characterized by a negative reflection coefficient;
- fault location: the reflection coefficient of the extremity where the fault is occurring is close to -1, as the fault impedance value can be assumed lower than the line surge impedance.

With the above illustrated assumptions and for a given network topology, it is possible to determine a certain number p of paths each one delimited between two extremities: Fig 1 shows these paths for a simplified network topology composed by a main feeder and a lateral. An observation point m where voltage or current waveforms are measured will see a certain number of paths p^* covered by the travelling waves. By making reference to Fig. 1 and to the observation point m placed at of Bus 01, such an observation point is able to see three paths, namely #01, #04 and #05.

The identification of these paths is clearly associated to the identification of both faulted branch and fault location.

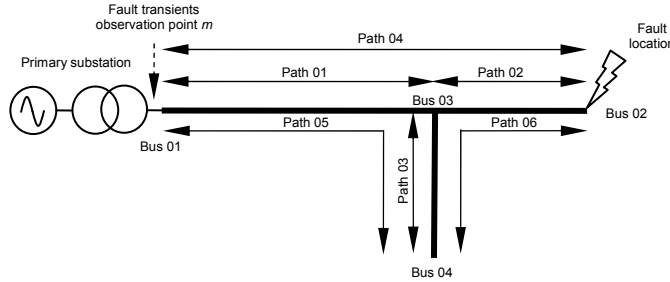


Fig. 1 – Paths covered by travelling waves caused by a fault at Bus 02.

As illustrated in [12], each path p can be associated to a number of characteristic frequencies, one for each of the travelling-wave propagation modes [15,16]. Indeed, it is worth noting that the propagation of travelling waves in multi-conductor lines involves the presence of different propagation speeds. Therefore, the identification of characteristic frequencies related to each path p is separately carried out for the various propagation modes. In order to apply the modal transformation matrixes in time domain, the modal transformation matrix should be real and their calculation in this paper is performed using the line constant routine of the EMTP [16].

Assuming that the network topology and travelling wave speeds of the various propagation modes are known, frequency $f_{p^*,i}$ of mode i through path p can be evaluated a priori as:

$$f_{p^*,i} = \frac{v_i}{n_p L_p} \quad (1)$$

where v_i is the travelling speed of the i -th propagation mode, L_p is the length of the p -th path and $n_p (\in \mathbf{N})$ is the number of times needed for a given travelling wave to propagate along path p before attain again the same polarity. $p-1$ values are used to identify the faulted section and the remaining ones to identify the fault distance between observation point m and the fault location. In particular, by referring to the example of Fig. 1, frequencies associated to paths #01 and #05 are used to identify the faulted branch and the frequency associated to path #04 to the fault location.

In order to clarify the concepts above illustrated, let us make reference to the results obtained on a reduced-scale experimental setup aimed at reproducing the fault-transient responses of

single-phase cable feeders. The scale factor is of 1:50. Fig. 2 shows one of the topologies adopted in [17] composed by a 1-km long main feeder with a 250-m long lateral branch connected at the middle of the main. All cable lengths are divided by this scale factor whilst the frequency of the power supply is multiplied by the scale factor in order to keep constant the ratio between the feeding voltage wavelength and the cable lengths. The reduced-scale cable lengths are reported in Fig. 2, along with the real-scale ones, in parenthesis. The equivalent reduced-scale power supply frequency, for a real-scale rated frequency of 50 Hz, is equal to 2.5 kHz. The cable lines are emulated by a single standard RG58 shielded cable, characterized by a 50Ω surge impedance and a measured inner-to-shield propagation speed of $1.786 \cdot 10^8$ m/s. The feeding voltage is provided by an Agilent 33120A function generator placed in series with a lumped $10 \text{ k}\Omega$ impedance in order to represent, as a first approximation, the primary substation transformer response to incoming fault-generated travelling waves.

The fault between the cable shield and its inner conductor is generated by means of a fast TTL-controlled micro-switch triggered by a National Instruments 9401 high-speed digital I/O board. The fault-originated waveforms are recorded at a single point located at the junction between the cable feeder and the $10 \text{ k}\Omega$ lumped impedance; this measurement point represents, in the real scale, the medium voltage side of the primary substation transformer. The signals are recorded by means of a LeCroy LT264 8-bit digital oscilloscope operating at the sampling frequency of 1 GHz.

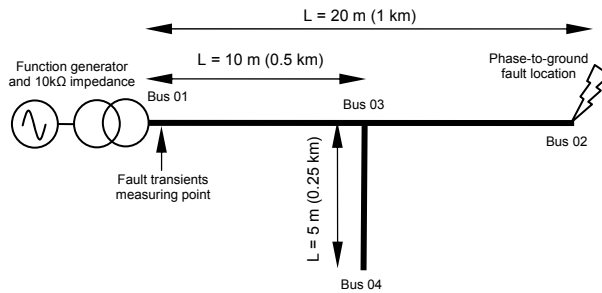


Fig. 2 – Topology of the a reduced scale setup aimed at reproducing electromagnetic fault transients. Adapted from [17].

Fig. 3 shows the fault-originated voltage transients, measured at Bus 01 shown in Fig. 2 and originated by a inner-to-shield fault. It can be observed that, as the fault triggered by the TTL micro-switch can be assumed as a step-function source, the voltage transients of Fig. 2 can be seen as the result of the superposition of different square waves, each one having a fundamental frequency given by (1), in addition to the steady state voltage waveform. Table I shows the theoretical frequencies observed at Bus 01 of Fig. 2 obtained by applying (1) to the considered network configurations.

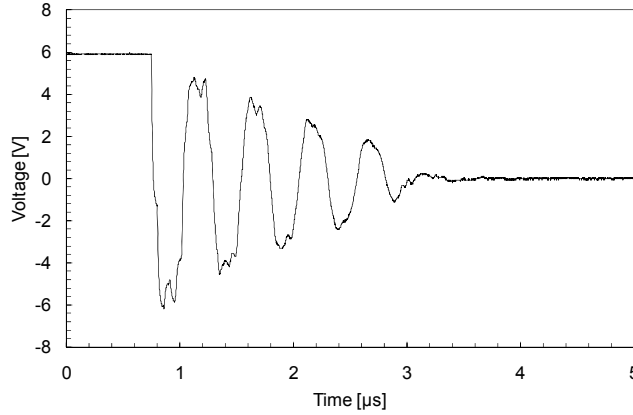


Fig. 3 – Reduced scale voltage transients measured in correspondence of the Bus 01 of the reduced scale model with the topology shown in Fig. 2. Adapted from [17].

Table I – Characteristic frequencies relevant to the propagation paths of topologies reported in Fig. 2 (reduced scale cable length). Adapted from [17].

| Path | Path length $n_p \cdot L_p$ [m] | Theoretical frequencies $f_{p,i}$ (inner-to-shield cable traveling speed equal to $1.786 \cdot 10^8$ m/s) |
|-----------|------------------------------------|--|
| | | [MHz] |
| Bus 01-02 | 4x20 (np=4) | 2.233 |
| Bus 01-03 | 4x10 (np=4) | 4.465 |
| Bus 01-04 | 2x15 (np=2) | 6.953 |

3. USE OF THE CONTINUOUS WAVELET TRANSFORM FOR THE IDENTIFICATION OF THE FAULTED BRANCH AND THE FAULT LOCATION

Current or voltage fault transient signals are composed by the superimposition of the industrial frequency waveform (constant low frequency component of large duration) and the transient disturbance caused by the fault (time-varying high frequency component of short duration). The resulting signal is therefore characterized by a continuous spectrum due to its time-variant properties. The identification of characteristic frequencies $f_{p,i}$ by means of traditional transformations, such as the Fast Fourier Transform (FFT), is certainly not appropriate. Indeed, such an operator analyzes the signal with a constant frequency resolution that depends to the width of the chosen observation time window.

In view of the above, the identification of characteristic frequencies $f_{p,i}$ should be accomplished by using appropriate signal analysis techniques that allow the adjustment of the signal spectrum versus time. Such a requirement is fulfilled by implementing the so-called time-frequency representations (TFRs) [18]. In particular, a signal TFR links a one-dimensional time signal $x(t)$ into a bi-dimensional function of time and frequency, $T_x(t,f)$. Typical examples of linear TFRs are the Short Time Fourier Transform (STFT) and the Wavelet Transform.

As known, for STFT, similarly to FFT, the time-frequency resolution is constant and equal to the duration of each subinterval adopted to divide the observed signal. Therefore, it is not the more appropriate tool for the analysis of fault transients.

The wavelet transform, on the other hand, is a TFR, which allows a good frequency resolution at low frequencies and a good time resolution at high frequencies [19]. In particular, it allows for the analysis of high frequency components very close in time to each other and for low frequency components very close to each other in frequency. These properties are indeed suitable for the study of transient waveforms produced by faults.

The fault location here adopted is based on the use of the CWT. As known, such a transformation applied to a signal $x(t)$ provides the integral of the product between $x(t)$ and the so-called daughter-wavelets, which are time translated and scale expanded/compressed

versions of a finite energy function $\psi(t)$, called mother wavelet. This transform, equivalent to a scalar product, produces wavelet coefficients $C(a,b)$ representing the TFR bi-dimensional function of time and frequency $T_x(t,f)$. Coefficients $C(a,b)$ can be seen as similarity indexes between the signal and the so-called daughter wavelet located at position b (time shifting factor) with scale a .

The analyzed part $s(t)$ of the recorded signal $x(t)$, which corresponds to a voltage or current fault-transient, is usually characterized by a short duration of few milliseconds. Such a duration corresponds to the product between the sampling time T_s and number of recorded samples N . Therefore, in the numerical implementation of the CWT applied to the signal $s(t)$, the elements of matrix $C(a,b)$ of are given by:

$$C(a,b) = C(a, iT_s) = T_s \frac{1}{\sqrt{|a|}} \sum_{n=0}^{N-1} \psi^* \left[\frac{(n-i)T_s}{a} \right] s(nT_s) \quad (2)$$

where parameter a corresponds to the scale factor, and product $i \cdot T_s$ corresponds to the time shifting factor b . It is worth nothing that if the center frequency of the mother wavelet $\psi(t)$ is F_0 , the one of the daughter-wavelet $\psi^*(at)$ is F_0/a .

The sum of the squared values of all coefficients belonging to the same scale, which are denoted as CWT signal energy $E_{CWT}(a)$, identifies a so-called ‘scalogram’ which provides the weight of each frequency component [20]:

$$E_{cwt}(a) = \sum_{n=0}^{N-1} (C(a, nT_s))^2 \quad (3)$$

It is important to note that the use of classical mother wavelets (e.g. the Morlet one) does not allow, in general, the identification of all the frequencies associated to the fault-originated travelling waves paths. As shown in [12], this limitation can be overcome by means of an appropriate definition of the mother wavelet, which, in order to maximize the similarity indexes between the analyzed signal and the daughter-wavelet, can be inferred from the fault transient itself, as proposed in [12].

The identification of the characteristic frequencies $f_{p^*,i}$ associated to the fault location was realized by inspecting the relative maximum peaks of the obtained scalogram $E_{CWT}(a)$ provided by (3). Such an approach disregards the information provided by the CWT time decomposition; they can however be used to successfully locate the fault too, as proposed in [8,9].

The improvement introduced by the method here illustrated is due to the integrated time-frequency analysis which involves a two-step identification of the characteristic frequencies.

The first step consists of an initial estimation of such frequencies $f_{p^*,i}$ as done in [12]. The second step improves the initial estimate by identifying the time differences between local maxima of the signal coefficients $C(a,b)$, defined by (2), in a specific frequency range centered in correspondence of the frequency $f_{p^*,i}$ identified by the first step.

Let consider the reduced scale network topology shown in Fig. 2 and the relevant fault transients of Fig. 3. Fig. 4 shows the scalogram of the signal energy values $E_{CWT}(a)$ obtained using equation (3) to coefficients $C(a,b)$ determined by means of the procedure described [12]. The identified frequencies are shown in Table II. These results show that the error in the identified characteristic frequency for the given fault location is equal to 11.3 % and a fault location error equal to 12.7 %.

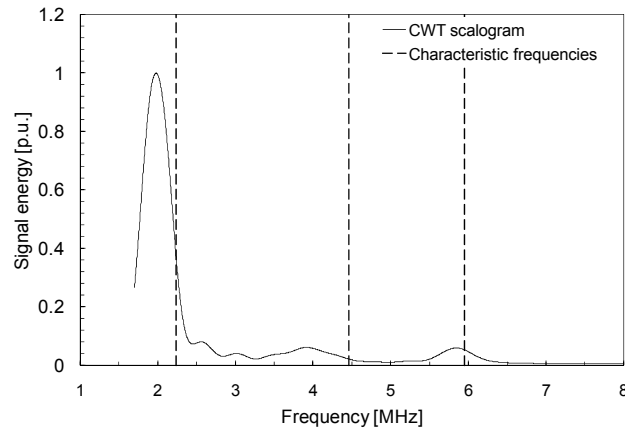


Fig. 4 – Energy scalogram relevant to the CWT analysis of the fault transient of Fig. 3 relevant to the single cable configuration of Fig. 2. Adapted from [17].

Table II – Characteristic frequencies relevant to the propagation paths of topologies reported in Fig. 2 (reduced scale cable length). Adapted from [17].

| Path | Path length $n_p \cdot L_p$ [m] | Theoretical frequencies $f_{p,i}$ (inner-to-shield cable traveling speed equal to $1.786 \cdot 10^8$ m/s) [MHz] | CWT identified frequencies $f_{p,i}$ by using the $E_{CWT}(a)$ [MHz] |
|-----------|---------------------------------|---|--|
| Bus 01-02 | 4x20 (np=4) | 2.233 | 1.980 |
| Bus 01-03 | 4x10 (np=4) | 4.465 | 3.922 |
| Bus 01-04 | 2x15 (np=2) | 6.953 | 5.844 |

Fig. 6 shows the analysis for the identification of time differences between local maxima of the coefficients $C(a,b)$ in the frequency range centered in the first-step identified frequency $f_{p,i}^* = 1.980$ MHz that corresponds to the fault location path (Bus 01 - Bus 02 of Fig. 2).

By making reference to this frequency, Fig. 5 shows coefficients $C(a,b)$ in the frequency range surrounding $f_{p,i} = 1.980$ MHz with a $\Delta f = 0.25$ MHz, which allows to identify a time difference of $0.490 \mu\text{s}$ corresponding to a characteristic frequency of 2.04 MHz. This yields a frequency error reduction of 8.6% and a fault location error of 9.3% . These values, which may appear somewhat large, are instead to be interpreted as reasonably small, in view of the reduced scale environment within which they have been inferred.

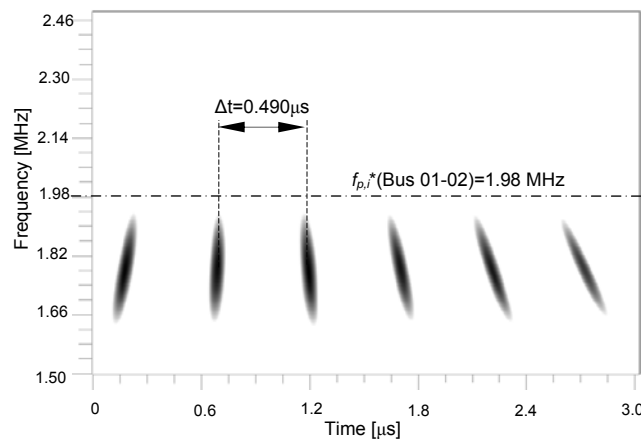


Fig. 5 – Coefficients $C(a,b)$ obtained by means of the CWT analysis applied to the fault transient of Fig. 3: improved estimation of the characteristic frequency associated with the faulted path between Buss 01-02.

Adapted from [17].

4. PROTOTYPE OF AUTOMATIC SYSTEM FOR THE FAULT LOCATION IN URBAN CABLE FEEDERS

The fault location procedure above described has been implemented into a test prototype of an automatic fault locator system. The relevant characteristics and performances are illustrated below.

The structure of the system is based on a modified version of a similar one developed for the automatic measurement of lightning-originated transients in power distribution networks [21]. In particular, each phase voltage transient is measured by means of voltage-to-voltage transducers (VVT) whose outputs are sent both to an event detection block and to an acquisition and A/D conversion board. This last board can operate, with simultaneous sampling, up to 100 MSa/s at 8 bits per channel, although its sampling rate has been set up at 10 MSa/s and the relevant recording time window has been fixed at 1 ms.

Concerning the event detection block above mentioned, it has been specifically designed to detect voltage transients superimposed to the industrial frequency voltage waveform [22]. As output, it provides a logic TTL signal that, in correspondence of a transient, acts as a trigger for the A/D conversion board.

Considering that analyzed fault transients are characterized by a rather large frequency spectrum, the VVT needs to be characterized by a relative large bandwidth. In order to satisfy such a requirement, the selected VVT is composed by a compensated capacitive voltage divider based on the Pearson Electronics VD305-A type and Fig. 6 shows the results of the experimental determined transfer function (dividing ratio and the phase shift) in the frequency range between 10 Hz ÷ 10 MHz. For each analyzed frequency, 50 measurements have been performed: the cross marks of Fig. 6 represent the mean values, whilst the vertical bars the 95% confidence interval.

The dividing ratio of each VVT (see the solid horizontal line in Fig. 6a) is estimated as the mean of the maximum and minimum values of the transfer function confidence intervals within 1 kHz ÷ 1 MHz (dotted horizontal lines in Fig. 6a). Concerning the phase of the VVT transfer function, it can be seen from Fig. 2b that, within the considered frequency range, namely 1 kHz ÷ 1 MHz, the phase shift is close to zero.

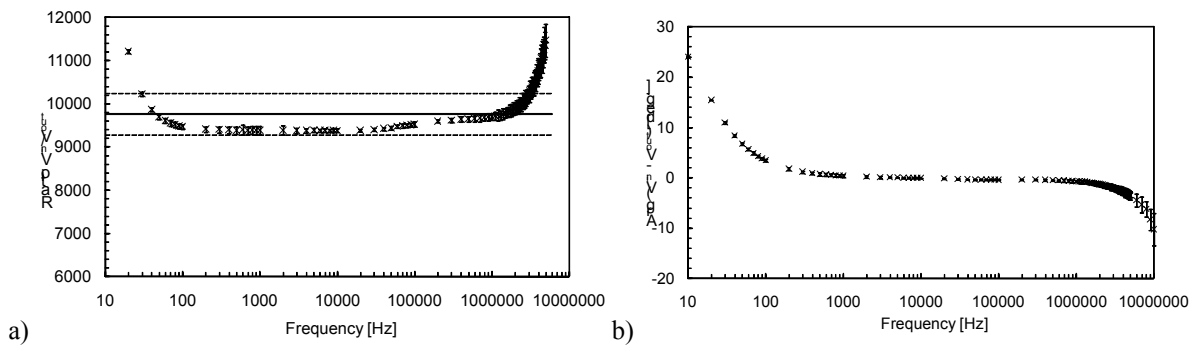


Fig. 6 – Example of the experimentally determined VVT transfer function: a) dividing ratio V_{in}/V_{out} ; b) phase-shift. Adapted from [21].

In order to experimentally validate the performances of the fault locator prototype, it has been decided to inject into the system – in particular in correspondence of the output voltages of the VVT – voltage transients whose waveforms has been previously calculated using an EMTP model and then reproduced by means of analog signal generators.

In particular, as the developed prototype is planned to be installed into a urban power distribution system characterized by the presence of single-cable feeders only, the EMTP

model has been conceived to represent such a condition. Fig. 7 shows the simulated power system within the EMTP-RV environment [23-25].

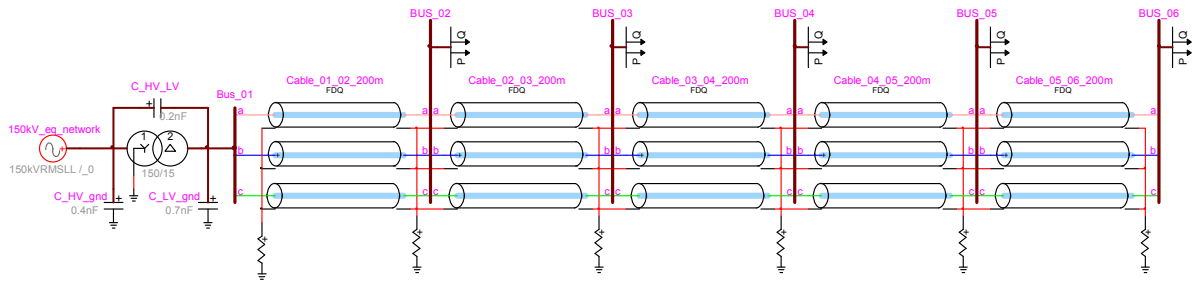


Fig. 7 – EMTP-RV model adopted to obtain fault transient waveforms in correspondence of the Bus_01.

The considered distribution system represents the primary 150/15 kV substation characterized by a 5 MVA power transformer, for which the relevant Π of capacitances has been also represented. It feeds a 1 km single-cable feeder composed by a three-phase ‘elicord-type’ EPR 12/20 kV shielded cable characterized by the data reported in Table III. Each 200 m, a secondary distribution substation is considered with its 15/0.4 kV power transformer (the relevant Π of capacitances of which have been also taken into account).

As it can be seen from Table III, the six propagation modes of the cable can be classified, as expected, in the following way: three inner-to-shield similar propagation modes, two similar shield-to-shield ones and a shields to ground one. As the majority of faults will occur between the inner and the shield conductor, only the characteristics relevant to the inner-to-shield propagation modes have been taken into account for the identification of the $f_{p*,i}$.

Table III – Characteristics of the power distribution cables of the simulated distribution system represented in Fig. 7.

| Geometry and material characteristics | | | | | | |
|--|----------------------------------|------------------|------------------|----------------------------------|-----------------------|------------------------|
| Inner conductor | | Shield | | | Insulation | |
| Ext. radius [mm] | Resistivity [$\Omega \cdot m$] | Int. radius [mm] | Ext. radius [mm] | Resistivity [$\Omega \cdot m$] | Relative permittivity | Insulation loss factor |
| 7.9 | $0.268 \cdot 10^{-7}$ | 13 | 13.3 | $0.173 \cdot 10^{-8}$ | 2.6 | 0.001 |
| Propagation modes (calculated at 10 kHz) | | | | | | |
| n. | Surge impedance [Ω] | | | Propagation speed [km/s] | | |
| 1 | 9.745 | | | $1.742 \cdot 10^5$ | | |
| 2 | 9.802 | | | $1.748 \cdot 10^5$ | | |
| 3 | 9.746 | | | $1.742 \cdot 10^5$ | | |
| 4 | 77.923 | | | $1.638 \cdot 10^4$ | | |
| 5 | 15.034 | | | $8.483 \cdot 10^4$ | | |
| 6 | 15.061 | | | $8.468 \cdot 10^4$ | | |

Concerning the fault transients, five locations have been considered in correspondence of each of the secondary substations, namely at 200 m, 400 m, 600 m, 800 m and 1000 m. Fig. 7 shows an example of fault transients observed at Bus_01, where the measurement point is placed, due to a phase-to-shield fault of phase a in correspondence of Bus_05. The high-frequency voltage transients involve, as expected, the faulted phase and, as they are measured within a time window of 1 ms, are not affected by pre and post fault steady state quantities. Therefore, the fault location procedure can be considered as independent from the presence of distributed generation.

The voltage transient signals observed in correspondence of Bus_01 and associated to each phase and to each of the selected fault locations are then transferred to three HP 33120A analog function generators aimed at reproducing the signals with an output sampling rate of 10 MHz. It is worth noting that, in order to synchronize the function generators, an external high speed TTL trigger signal is provided to the three devices by means of a National Instruments 9401 board (100 ns rise time).

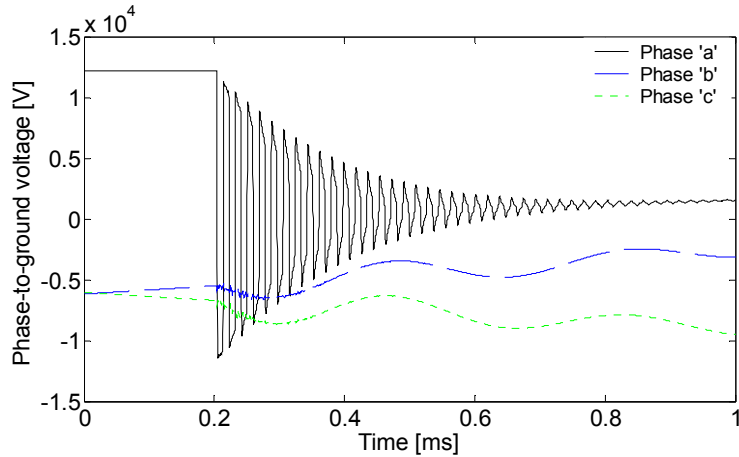


Fig. 8 – EMTP-RV model adopted to obtain fault transient waveforms in correspondence of the Bus_01.

Table IV contains a summary of the performances of the developed fault location prototype with reference to the five considered fault locations. Theoretical and identified frequencies along with fault location errors are reported too. Concerning this last quantity, it has been estimated, as done in [12], by means of the following equation

$$e_{\%} = \frac{100}{L_p} \left| L_p - \frac{v_i}{n_p \cdot f_{p^*,i}^{CWT}} \right| \quad (4)$$

where: L_p is the length of the path associated to the fault location.

As it can be seen from the results of Table IV the fault location errors are contained within 2 meters, which means fault location errors lower than 1%.

Table IV – Fault location paths, relevant theoretical and identified characteristic frequencies and fault location errors with reference to the distribution system of Fig. 7.

| Path | L_p [m] | n_p | Theoretical frequencies $f_{p^*,i}$ (inner-to-shield cable travelling speed equal to $1.742 \cdot 10^8$ m/s) [kHz] | CWT identified frequencies $f_{p^*,i}$ [kHz] | Frequency identification error [kHz] | Fault location [m] | Fault location error% [%] |
|-----------------|-----------|-------|--|--|--------------------------------------|--------------------|---------------------------|
| Bus_01 – Bus_02 | 200 | 4 | 217,69 | 215,8 | 1,89 | 201,70 | 0,85 |
| Bus_01 – Bus_03 | 400 | 4 | 108,85 | 108,4 | 0,45 | 401,62 | 0,41 |
| Bus_01 – Bus_04 | 600 | 4 | 72,563 | 72,4 | 0,163 | 601,18 | 0,20 |
| Bus_01 – Bus_05 | 800 | 4 | 54,422 | 54,4 | 0,022 | 800,21 | 0,03 |
| Bus_01 – Bus_06 | 1000 | 4 | 43,538 | 43,6 | 0,062 | 998,54 | 0,15 |

5. CONCLUSIONS

An accurate fault location procedure has been presented, which is based on the analysis of high frequency transients associated to the travelling wave phenomena occurring after a fault event into power distribution networks. The theoretical background concerning the problem of correlating the fault location to specific paths and to characteristic frequencies, thus allowing the identification of both faulted branch and fault location has been covered.

The paper has then discussed the identification of these characteristic frequencies: the continuous wavelet analysis applied to fault transients has been proved to be a suitable tool for solving the problem of interest. A first experimental validation of the effectiveness of the proposed procedure has been accomplished by means of a reduced scale cable distribution system.

The paper has eventually illustrated the implementation of the proposed procedure into a fault locator prototype, which structure has been defined on the basis of the experience previously gained through the development of system for the measurement and acquisition of fast overvoltage transients in power networks. The performance assessment of the prototype has been accomplished experimentally by using real-time generated analog voltage waveform transients previously calculated by means of an EMTP model representing typical single cable feeders of urban distribution networks. The result of these tests has allowed us to conclude that, with reference to the considered network configuration, the fault location errors of the developed prototype are within 2 meters, with relevant percent fault location errors lower than 1%.

BIBLIOGRAPHY

- [1] CIRED WG03 Fault management, "Fault management in electrical distribution systems", 1998.
- [2] IEEE Std C37.114, "IEEE guide for determining fault location on AC transmission and distribution lines", 2004.
- [3] M. S. Sachdev and R. Agarwal, "A technique for estimating transmission line fault locations from digital impedance relay measurements" IEEE Trans. on PWRD, vol. 3, no. 1, pp. 121–129, Jan. 1988.
- [4] K. Srinivasan and A. St.-Jacques, "A new fault location algorithm for radial transmission lines with loads," IEEE Trans. on PWRD, vol. 4, no. 3, pp. 1676–1682, Jul. 1989.
- [5] A. A. Girgis, D. G. Hart, and W. L. Peterson, "A new fault location technique for two- and three-terminal lines," IEEE Trans. on PWRD, vol. 7, no. 1, pp. 98–107, Jan. 1992.
- [6] G. B. Ancell and N. C. Pahalawatha, "Maximum likelihood estimation of fault location on transmission lines using travelling waves," IEEE Trans. on PWRD, vol. 9, no. 2, pp. 680–689, Apr. 1994.
- [7] O. Chaari, M. Meunier, and F. Brouaye, "Wavelets: A new tool for resonant grounded power distribution systems relaying," IEEE Trans. on PWRD, vol. 11, no. 3, pp. 1301–1308, Jul. 1996.
- [8] F. H. Magnago and A. Abur, "Fault location using wavelets," IEEE Trans. on PWRD, vol. 13, no. 4, pp. 1475–1480, Oct. 1998.
- [9] F. H. Magnago and A. Abur, "A new fault location technique for radial distribution systems based on high frequency signals," in Proc. IEEE-Power Eng. Soc. Summer Meeting, vol. 1, pp. 426–431, Jul. 18–22, 1999.
- [10] D. W. P. Thomas, R. E. Batty, C. Christopoulos, and A. Wang, "A novel transmission-line voltage measuring method," IEEE Trans. Instrum. Meas., vol. 47, no. 5, pp. 1265–1270, Oct. 1998.
- [11] A. Borghetti, S. Corsi, C. A. Nucci, M. Paolone, L. Peretto, and R. Tinarelli, "On the use of continuous-wavelet transform for fault location in distribution power networks," Elect. Power Energy Syst., vol. 28, pp. 608–617, 2006.
- [12] A. Borghetti, M. Bosetti, M. Di Silvestro, C.A. Nucci and M. Paolone, "Continuous-Wavelet Transform for Fault Location in Distribution Power Networks: Definition of Mother Wavelets

- Inferred from Fault Originated Transients”, IEEE Trans. on PWRS, vol. 23, No. 2, pp.380-388, may 2008.
- [13] Feng Yan, Zhiye Chen, Zhirui Liang, Yinghui Kong, Peng Li, “Fault location using wavelet packets”, Proc. of Int. Conf. on Power System Technology, PowerCon 2002, Vol. 4, pp. 2575 - 2579, 13-17 Oct. 2002.
 - [14] A. Greenwood, Electrical Transients in Power Systems, John Wiley and Sons, New YorkAJSJA, 1991.
 - [15] E. Clarke, Circuit analysis of AC power systems, 1. New York: John Wiley & Sons; 1943.
 - [16] H.W. Dommel, “Digital computer solution of electromagnetic transients in single and multi-phase networks”, IEEE Trans Power Apparatus Syst 1969;PAS-88(April):388–99.
 - [17] A. Borghetti, M. Bosetti, M. Paolone, A. Abur, “Integrated Use of Time-Frequency Wavelet Decompositions for Fault Location in Distribution Networks: Theory and Experimental Validation”, Proc. of the 2009 International Conference on Power Systems Transients, Kyoto, June 2-6 2009.
 - [18] A. V. Oppenheim, R. W. Schaffer, Discrete-time signal processing, Prentice Hall, Englewood Cliffs, NJ, USA, 1989.
 - [19] A. Graps, “An introduction to wavelets”, IEEE Computational Science and Engineering, vol. 2, n. 2, 1995, pp. 50-61.
 - [20] T. Lobos, T. Sikorski, P. Schegner, “Joint time-frequency representation of non-stationary signals in electrical power engineering”, Proc. of the 15th Power Systems Computation Conference (PSCC'05), Liege, Belgium, 22-26 August 2005, paper fp 97.
 - [21] K. Yamabuki, A. Borghetti, F. Napolitano, C.A. Nucci, M. Paolone, L. Peretto, R. Tinarelli, M. Bernardi, R. Vitale, “A Distributed Measurement System for Correlating Faults to Lightning in Distribution Networks”, Proc. of the International Symposium on High Voltage Engineering (ISH), Ljubljana, Slovenia, Aug. 27-31, 2007.
 - [22] L. Peretto, P. Rinaldi, R. Sasdelli, R. Tinarelli, A. Fioravanti, “A System for the Measurement of the Starting Instant of Impulsive Transients”, IEEE Trans on Instrumentation and Measurement, vol. 56, 2007, pp. 1955-1960.
 - [23] J. Mahseredjian, S. Lefebvre and X.-D. Do, “A new method for time-domain modelling of nonlinear circuits in large linear networks”, Proc. of 11th Power Systems Computation Conference PSCC, August 1993.
 - [24] J. Mahseredjian, S. Denetière, L. Dubé, B. Khodabakhchian and L. Gérin-Lajoie: “On a new approach for the simulation of transients in power systems”. Electric Power Systems Research, Vol. 77, Issue 11, September 2007, pp. 1514-1520
 - [25] J. Mahseredjian: “Simulation des transitoires électromagnétiques dans les réseaux électriques”, Édition ‘Les Techniques de l'Ingénieur’, Dossier n°D4130, Réseaux électriques et applications..